Journal of Alloys and Compounds 960 (2023) 170686

Contents lists available at ScienceDirect

Journal of Alloys and Compounds

journal homepage: www.elsevier.com/locate/jalcom

Research Article

Improved ductility of annealed Fe-based metallic glass with good soft magnetic property by cryogenic thermal cycling

Siyi Di [a,b,c], Jing Zhou [d], Mingjuan Cai [c], Jingxian Cui [c], Xuesong Li [d], Baolong Shen [c], Haibo Ke [d,*], Qianqian Wang [c,*]

[a] State Key Laboratory of Metal Matrix Composites, Shanghai Jiao Tong University, Shanghai 200240, China
[b] School of Materials Science & Engineering, Shanghai Jiao Tong University, Shanghai 200240, China
[c] School of Materials Science and Engineering, Jiangsu Key Laboratory for Advanced Metallic Materials, Southeast University, Nanjing 211189, China
[d] Songshan Lake Materials Laboratory, Dongguan 523808, China

ARTICLE INFO

Article history:
Received 2 December 2022
Received in revised form 24 April 2023
Accepted 20 May 2023
Available online 22 May 2023

Keywords:
Fe-based metallic glass
Annealing brittleness
Magnetic property
Cryogenic thermal cycling

ABSTRACT

The brittleness after annealing treatment severely restricts the subsequent processing and application of Fe-based magnetic metallic glass. Through proper annealing treatment combined with cryogenic thermal cycling, we obtained excellent comprehensive properties of Fe-based metallic glass ribbons with not only good soft magnetic properties but also high bending deformation ability. After thermal cycling, the sample rejuvenated with higher energy state and larger size of soft regions, which facilitated the initiation and branching of shear bands, leading to the improvement of bending plasticity. Although the large soft regions may act as pining sites for domain walls, the domain structure and coercivity of the sample remained nearly identical because of the reduced number of crystal-like structures. Our study indicates that the cryogenic thermal cycling is an effective method to regulate mechanical and magnetic properties, which makes it powerful means to obtain excellent performance of Fe-based magnetic metallic glasses.

1. Introduction

Fe-based metallic glasses (MGs) have aroused great interests due to their excellent soft magnetic properties, such as high saturation magnetic flux density (B_s), low coercivity (H_c), and low core loss [1–3]. Annealing below the crystallization temperature is an essential step to release residual stress during manufacturing and obtain better soft magnetic properties for Fe-based MGs [4]. However, this process accelerates the structural relaxation of amorphous matrix and often leads to a sharp deterioration of plasticity, which brings huge inconvenience to subsequent processing [5]. Numerous researches have been carried out to reduce the brittleness of Fe-based magnetic MGs after annealing, such as composition modification and flash annealing technology [5–7]. It has been found that adding elements with high Poisson's ratio, such as Ni/Mo, can effectively increase the ductile-brittle transition temperature and reduce the brittleness after annealing [6]. Nevertheless, this method is usually accompanied by sacrificing the soft magnetic properties or glass-forming ability. The flash annealing technology also has some drawbacks, for example, it has specific requirements on heating equipment, ribbon width and oxidation resistance of the alloys, which is not applicable to all the Fe-based MG systems.

Recently, it has been proved that rejuvenation is an effective method to improve the plastic deformation capacity of MGs [8,9]. Rejuvenation is the reverse state of relaxation, corresponding to higher energy state and more disordered structure of MGs. Compared with some mechanical approaches to realize rejuvenation, cryogenic thermal cycling (CTC) method, which subjects samples to cycling between thermal and cryogenic temperatures has attracted more attention [10]. This method is easy to be carried out and has no limitation on sample size. Particularly, it seems that it is barely detrimental on soft-magnetic properties of Fe-based MGs [11,12]. In previous study, the CTC treatment has been reported to effectively improve the compressive and tensile plasticity of the as-cast $[(Fe_{0.5}Co_{0.5})_{0.75}B_{0.2}Si_{0.05}]_{96}Nb_4$ MG samples [13,14]. However, whether the CTC treatment can make sense on annealed samples is still unknown. It has been suggested that the rejuvenation effect of CTC is caused by internal stress during thermal cycling, attributed by local differences of thermal expansion coefficient [10,15]. The initial amount of heterogeneity before CTC treatment seems to play an important role, heterogeneous MGs with nano-sized clusters and free volumes are more affected by CTC treatment than the

* Corresponding authors.
E-mail addresses: kehaibo@sslab.org.cn (H. Ke), qwang678@seu.edu.cn (Q. Wang).

https://doi.org/10.1016/j.jallcom.2023.170686
0925-8388/

homogeneous ones [16–18]. While during annealing treatment, the relaxation behavior often accompanies with the annihilation of free volumes and leads to a uniform structure. Besides, although the CTC treatment seems to have no impact on soft magnetic properties, the underlying mechanism is not well understood, the effects on magnetic domain structures have rarely been reported and worth further exploration.

In this study, CTC combined with short-time annealing treatment were applied to $[(Fe_{0.5}Co_{0.5})_{0.75}B_{0.2}Si_{0.05}]_{96}Nb_4$ MG ribbons. After annealing with shorter time, free volumes and a non-uniform structure were retained. The size of soft regions became larger after CTC treatment, which facilitated the initiation and branching of shear bands (SBs), leading to the enhancement of bending plasticity strain. Despite the pinning effects of soft regions, the number of crystal-like ordering structures decreased, resulting in the slight decrease of H_c. As a result, the Fe-based MG ribbons with excellent soft magnetic properties and bending plasticity were obtained.

2. Experimental methods

Alloy ingots with nominal composition of $[(Fe_{0.5}Co_{0.5})_{0.75}B_{0.2}Si_{0.05}]_{96}Nb_4$ were prepared by induction melting a mixture of high-purity (> 99.9 wt%) constituent elements in a highly purified argon atmosphere. MG ribbons were prepared by melt spinning under an argon atmosphere. Samples with a length of 60 mm were isothermally annealed at 745 K (75 K below glass transition temperature, T_g) for different time of 5/10/15/18/20 min. Afterwards, CTC treatment was applied to these ribbons. In each cycle, the ribbons were firstly dipped into liquid nitrogen for 1 min, then immediately immersed in hot silicone oil for 1 min. A whole CTC treatment includes 15 cycles. The temperature of oil was set to be 473 K (0.58 T_g). The as-quenched, annealed with different time and CTC treated samples are denoted as AQ, AN5, AN10, AN15, AN18, AN20, CTC-AQ, CTC-AN5, CTC-AN10, CTC-AN15, CTC-AN18 and CTC-AN20 samples, respectively.

Bending tests were performed using a digital micrometer setup [11,19]. The ribbon samples were clamped between two micrometer platen faces. The micrometer screw was turned incrementally to smaller distances, resulting in a gradual increase in ribbon bending strain. The bending strain, ε, was evaluated by

$$\varepsilon = t/(d - t)$$

where t is the thickness of the ribbon and d is the fracture or buckling distance. When $d = 2t$, $\varepsilon = 1\,\%$ or 100 %, i.e., the ribbon has bent completely and doubled its thickness. Five individual bending tests were repeated for samples with specific treatments. The morphologies of the surface and vertical section after fracture were observed by scanning electron microscopy (SEM, Sirion 200, FEI). H_c was obtained with a *B-H* loop tracer (RIKEN BHS-40) under a maximum applied magnetic field of 1 kA/m. B_s was measured with a vibrating sample magnetometer (VSM, Lake Shore 7410) under a magnetic field up to 800 kA/m at room temperature. The domain structures of ribbons were confirmed using the Magneto-optical Kerr Microscope (MOKE, em-Kerr-highres). The phases of samples were examined by an X-ray diffractometer (XRD, D8-Discover, Bruker). The enthalpies of relaxation (ΔH_{rel}) for the samples were measured by differential scanning calorimeter (DSC, Netzsch 404 F3). The samples were heated to 973 K (above T_g) at a heating rate of 20 K/min, and then cooled to room temperature, followed by a second cycle using the same procedure. The ΔH_{rel} was calculated from the area difference between the first and second cycle curves below T_g. Five samples for each condition were tested to ensure the repeatability. High-resolution transmission electron microscopy (HRTEM, Talos F200X) analysis was carried out to observe the microstructure changes. The samples for HRTEM analysis were thinned by ion milling method (Gatan Inc., PIPS-M691) under liquid nitrogen cooling condition. For high angle annular dark-field (HAADF) imaging, a probe semi-convergence angle of 10.5 mrad and collection semi-angle of 58–200 mrad were used.

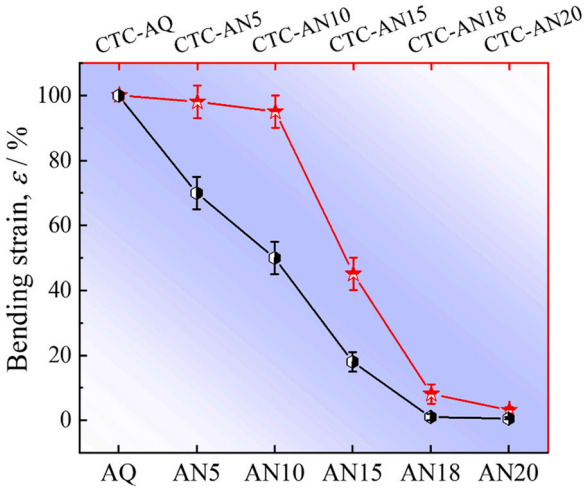

Fig. 1. Bending strains of the $[(Fe_{0.5}Co_{0.5})_{0.75}B_{0.2}Si_{0.05}]_{96}Nb_4$ MG ribbons before and after different treatments.

3. Results

3.1. Mechanical properties

The bending plastic strains (ε) of $[(Fe_{0.5}Co_{0.5})_{0.75}B_{0.2}Si_{0.05}]_{96}Nb_4$ MG samples after annealing and CTC treatments are shown in Fig. 1. Without annealing, the AQ and CTC-AQ samples exhibit no fracture or buckling behavior and remain totally intact and plastic. With the increase of annealing time, the ε of the ribbon sample decreases gradually. When the annealing time increases to 20 min, the ribbon fractures completely during bending test. The CTC processing applied after annealing seems to be beneficial to enhance the deformation ability. After CTC treatment, the ε of AN5 sample increases from 70 % to 98 %, and for AN10 sample, the ε increases more dramatically from 50 % to 95 %. The data for AN15 sample is from 18 % to 45 %, while for AN18 and AN20 samples, the increments are almost negligible. It is obvious the effectiveness of CTC treatment reduces with the prolongation of annealing time.

Fig. 2 shows the surface ((a–f)-1) and vertical section ((a–f)-2) morphology after bending fracture for the ribbon samples. It can be seen that the AN10, AN15, AN20, CTC-AN15 and CTC-AN20 samples show smooth surfaces without obvious SBs, indicating that the deformation is mainly controlled by single SB during bending. Once the main SB is formed, it will rapidly develop into crack across the entire ribbon, resulting in fast shear failure. In contrast, abundant secondary SBs are observed near the fracture edge of CTC-AN10 sample Fig. 2(b-1). The strain energy can be effectively released through the branching of multiple SBs, and the intersection between SBs is beneficial to inhibit fast shear failure [10,11,13,14]. As a result, the CTC-AN10 sample has higher bending plasticity. With increased annealing time, the vertical section morphology also demonstrates a ductile-brittle transition. For AN10, CTC-AN10 and CTC-AN15 samples, the vertical sections are relatively smooth and flat. The smooth morphology is related to the stable propagation of SBs and often corresponds to ductile deformation mechanism [20]. A few discontinuous floccules can also be observed at the edge, suggesting that adiabatic heating and local melting behavior occur at later stage of shear deformation, which leads to the instability [21]. For AN15, AN20 and CTC-AN20 samples, cleavage features with ridges and rivers are observed, especially for AN20 and CTC-AN20 samples,

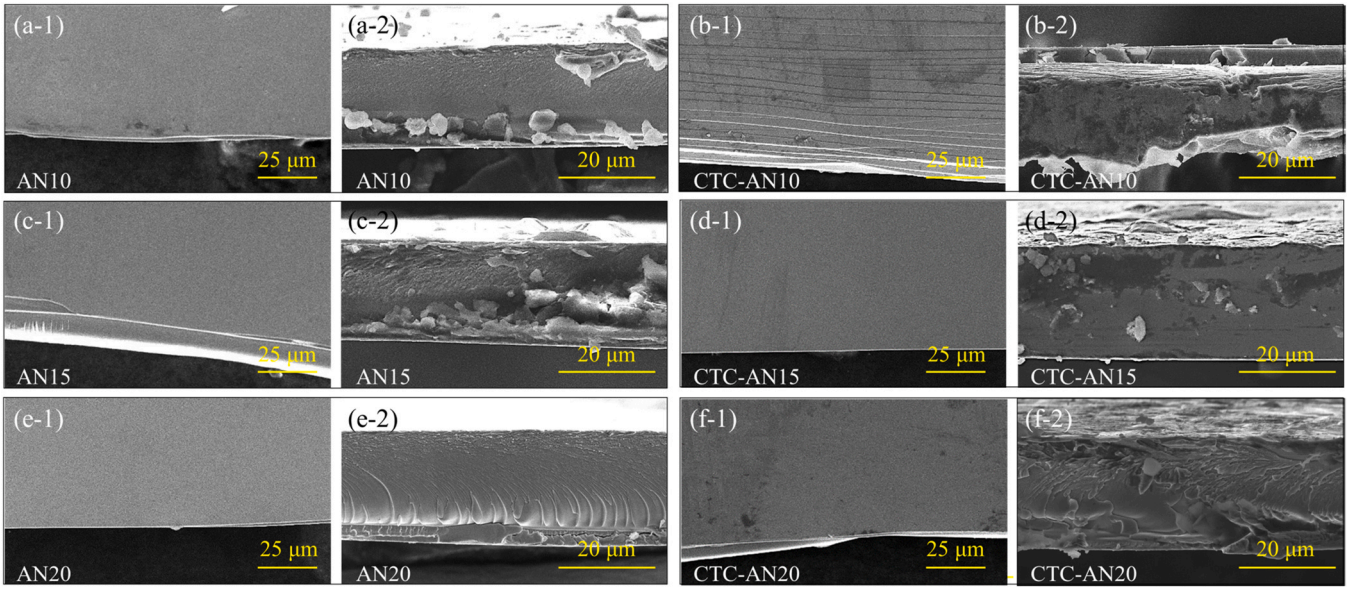

Fig. 2. The SEM images of surface and vertical section morphology after bending fracture for AN10, AN15, AN20, CTC-AN10, CTC-AN15 and CTC-AN20 samples.

indicating the brittle fracture behavior. When the temperature increases due to the adiabatic heating generated by large residual strain energy, the materials in SBs quickly turn into viscid matter, ridges and rivers instead of perfect veins are formed on the fracture surface, leading to catastrophic fracture [22]. Besides, different from the neat feature of fracture edges for other samples, the edge of the CTC-AN10 sample is more rugged and uneven, suggesting a slower release of elastic energy and better shear stability, which may account for the largest bending plasticity of this sample.

3.2. Soft magnetic performance and magnetic domain structure

The *B-H* curves of the AQ and treated samples under different conditions are shown in Fig. 3(a), with partly enlarged drawing of B_s as inset. The summary charts of H_c and B_s for the samples are shown in Fig. 3(b) and (c). After annealing, the B_s increases from 1.01 to 1.05 T, and H_c decreases sharply from 22.3 to 2.0 A/m. The enhancement of B_s may result from the structural relaxation during annealing treatment, which leads to a more uniform and dense structure [23]. The annealing treatment also releases the residual stress in the matrix, reducing pinning effects of domain walls from defects and thus facilitating magnetization or demagnetization. Therefore, the H_c decreases obviously after annealing. Compared with annealing, the effects of CTC treatment on soft magnetic properties are not significant, which is consistent with previous studies [11,12]. The B_s of CTC-AQ and CTC-AN10 samples decrease slightly compared with AQ and AN10 samples. For AN15 and AN20 samples, the B_s increase after thermal cycling, especially for AN20 sample, B_s increases from 1.05 to 1.06 T. After CTC treatment, the H_c increases from 8.3 A/m to 8.9 A/m for AN10 sample, and for AN15

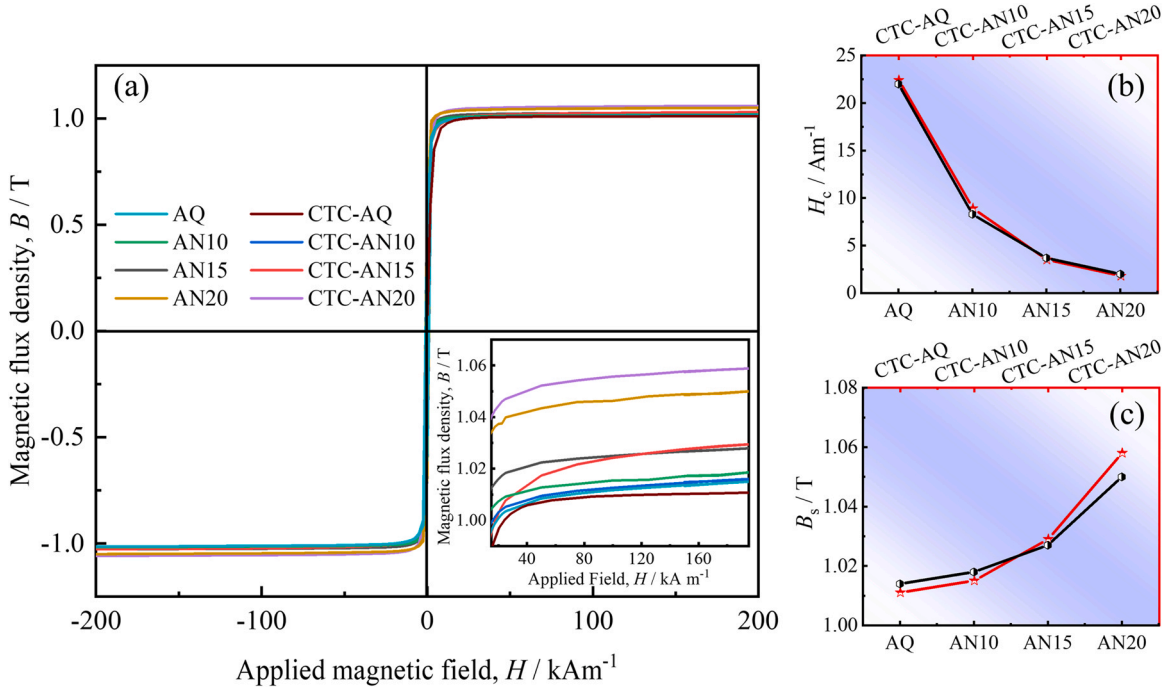

Fig. 3. (a) *B-H* curves, (b) H_c and (c) B_s of the AQ and treated samples, the inset in (a) is the partly enlarged drawing.

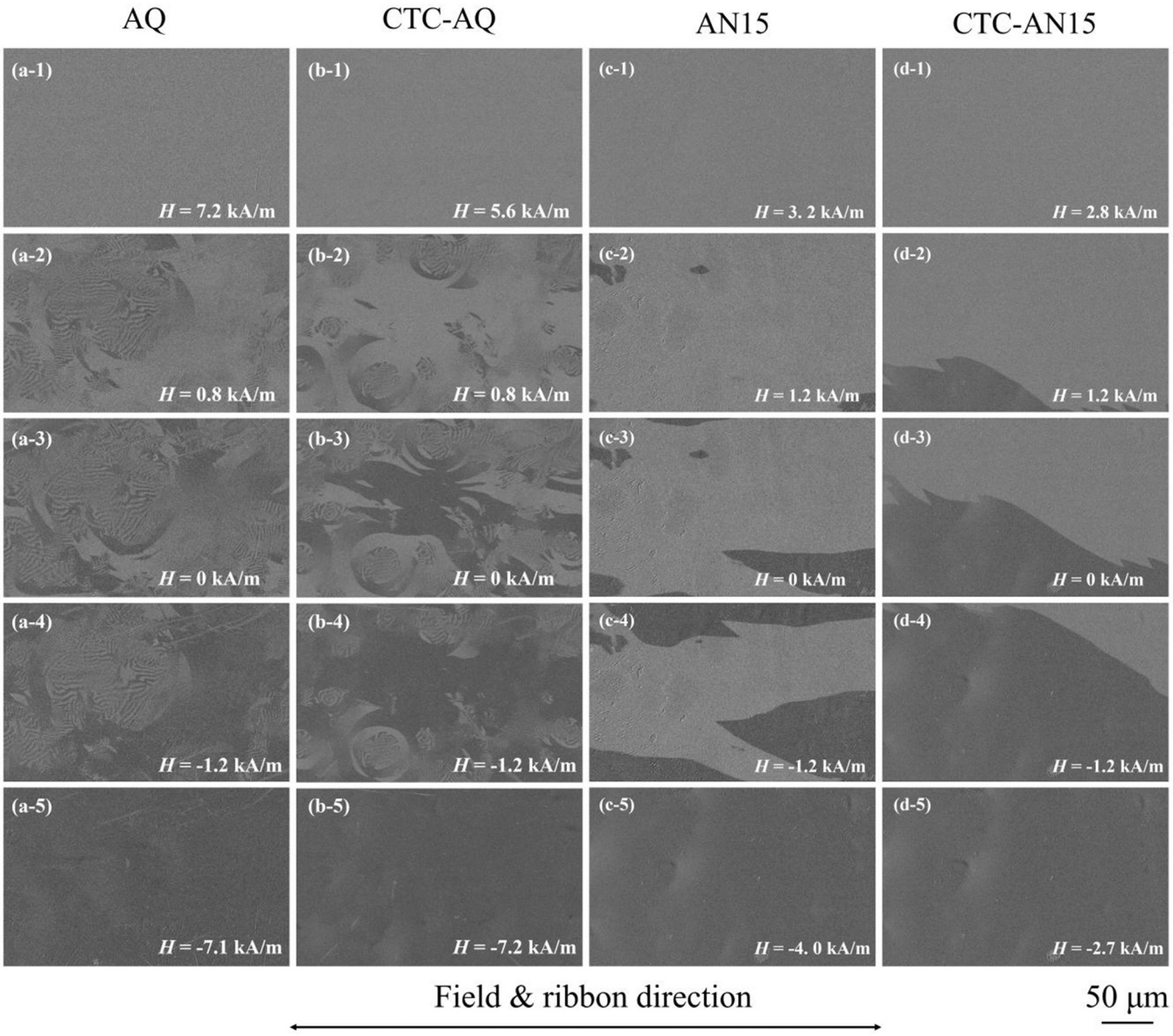

Fig. 4. The magnetization processes recorded under static field for (a) AQ, (b) CTC-AQ, (c) AN15 and (d) CTC-AN15 samples.

and AN20 samples, H_c decreases a little. After short-time annealing combined with CTC treatment, the CTC-AN15 sample exhibits excellent comprehensive properties with 45 % of bending strain, 1.03 T of B_s and 3.8 A/m of H_c.

To clarify the effect of annealing and CTC treatments on magnetic structure, in situ observation of the magnetic domains' evolution with a varying magnetic field were performed. Fig. 4 shows the magnetic domains of AQ, CTC-AQ, AN15 and CTC-AN15 samples under different static fields. The magnetization processes of AQ and CTC-AQ samples are controlled by both wall motion and moment rotation, manifested as wide-curved domains and fingerprint-like domains. The fingerprint-like domains nucleate early during the magnetization reversal and require higher field to get saturated compared with the wide-curved domains. According to the previous study, the strong residual stress in AQ samples will trigger in-plane and vertical magnetic anisotropy, effectively pinning the domain walls and restraining the wall propagation, leading to poor soft-magnetic properties [24–26]. After annealing for 15 min, the sample can reach complete magnetization at much lower magnetization field. The fingerprint-like domains almost disappear, and the wide-curved domains growing further with increasing strength of the negative field. After annealing for 15 min, most of the residual stress can be released, the structure becomes more homogeneous, which facilitates an unobstructed movement of the domains and leads to enhanced magnetic softness. However, the domain edges of AN15 and CTC-AN15 samples are not totally smooth, which means that the pinning effect also exists. It's worth noting that before and after CTC treatment, the domain structures of ribbon samples do not show significant differences, which illustrates the identical H_c after CTC treatment.

3.3. Thermal properties

The deformation capacity of MG is closely related to their free volume content and energy state, which can be indirectly reflected by the relaxation enthalpy (ΔH_{rel}) according to previous studies [10,27]. Fig. 5 shows the representative relaxation spectra and ΔH_{rel} with error bars of the AQ and treated samples. As the annealing time increases, the ΔH_{rel} gradually decreases, indicating the decreased number of free volume. This is because that annealing at high

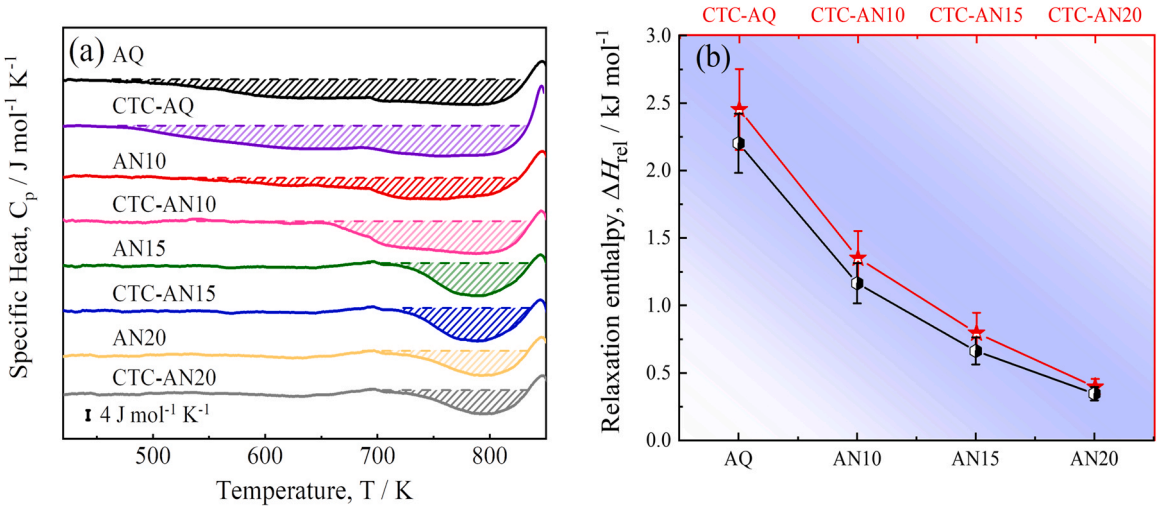

Fig. 5. The relaxation heat for the AQ and treated MG ribbons. (a) The typical relaxation spectra, (b) the variation of ΔH_{rel} with error bars.

temperature accelerates the relaxation process of MGs, accompanied by the homogenization of structure and annihilation of free volumes. After CTC treatment, the ΔH_{rel} increases to different extent. The CTC-AQ sample obtains the largest increase of ΔH_{rel}, while the CTC-AN20 sample shows almost negligible change. This is because the rejuvenation effect of CTC is caused by internal stress during thermal cycling, attributed by local variation of thermal expansion coefficient. After annealing for a long time, large number of free volumes are annihilated. In this case, the local stress is too small to cause large-scale atomic rearrangement, so the rejuvenation effect is not conspicuous. When the annealing time is relatively short, a certain number of free volumes can be retained in the alloy to form an inhomogeneous structure with the combination of hard and soft regions, which is easier to form a large local stress to induce atomic rearrangement during the CTC treatment.

The changes of ΔH_{rel} are consistent with that of deformation capacity. In general, the regions containing larger number of free volumes have lower local stiffness and stability, which can serve as fertile initiation sites for shear transformation zones (STZs) [28]. While for MG with a homogeneous and relaxed structure, the nucleation and percolation of STZs tend to be difficult, which results in the fast propagation of SBs and shear failure. The number of free volume in MG also affects H_c. The difficulty of domain wall movement and magnetic moment rotation, anisotropy and residual stress make great impact on H_c, and the most important factor is the pinning effect of internal stress sources on domain walls [24–26]. The free volume is similar to the point defect, which can act as a stress source to pin the magnetic domain and cause the increase of H_c. Nevertheless, the ΔH_{rel} of CTC-AN15 increases but H_c remains similar after thermal cycling, indicating that there exists other structural variation factor that impact on H_c.

3.4. Structure characterization

The phases of the AQ and treated samples were investigated by XRD measurements and all samples keep amorphous structure, as can be seen in Fig. 6. Fig. 7(a–c) are the HRTEM images of AQ, AN15 and CTC-AN15 samples, with the selected area electron diffraction (SAED) patterns shown in the insets. The diffuse halo rings in SAED patterns suggest that the amorphous structure remains after annealing and CTC treatment. Apart from the maze-like matrix, some crystal-like ordering (CLO) structures can also be seen. In order to quantitatively analyze the orderings, 2D autocorrelation function analysis is utilized [29,30]. Randomly selected regions of the HRTEM images of the three samples are divided into 100 square sub-cells

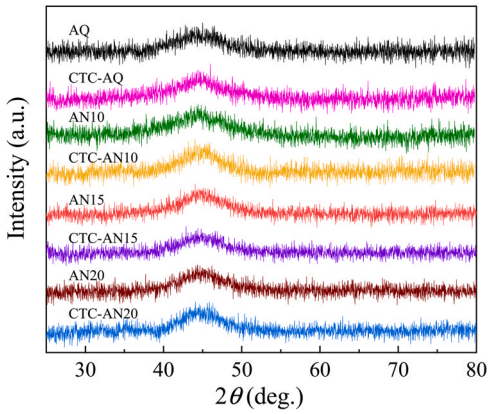

Fig. 6. XRD patterns of AQ and treated samples.

with a size of 1.028 nm × 1.028 nm, which is close to the size of CLOs. The resulting images are shown in Fig. 7(d–f). The total fraction of CLO structures is 14 % in AQ sample, 13 % in AN15 sample and 7 % in CTC-AN15 sample. During annealing treatment, the free volumes annihilate a lot, but the number of CLO structures remains almost constant, probably because the temperature is much lower than the crystallization temperature. For CTC-AN15 sample, the number of CLO structures decreases sharply, which means that about half of them are destroyed during CTC treatment. The destruction of CLOs during CTC treatment has also been reported in previous study of $\{[(Fe_{0.5}Co_{0.5})_{0.75}B_{0.2}Si_{0.05}]_{96}Nb_4\}_{99.9}Cu_{0.1}$ MG [12]. Ferromagnetic amorphous alloy has an Invar effect below Curie temperature (700 K in this paper), resulting in a smaller thermal expansion coefficient compared to its crystalline phase [31]. Therefore, CLOs with crystal-like structures can be easily influenced by thermal stress and are inclined to be destroyed during the expansion and contraction process.

The high-resolution HAADF-STEM images of the three samples are shown in Fig. 8(a–c), showing contrast with dark and bright areas, as a result of heterogeneous distributions of density and/or chemistry. As the elemental mappings (Fig. 8(d–f)) of three samples show homogeneous distributions, the dark-bright contrasts in HAADF images mainly arise from the density variations. According to the nano-beam electron diffraction observation, the bright regions correspond to matrix with relatively higher density and structure ordering, while the dark regions correspond to loosely packed regions with lower density and structure ordering [32]. It is obvious

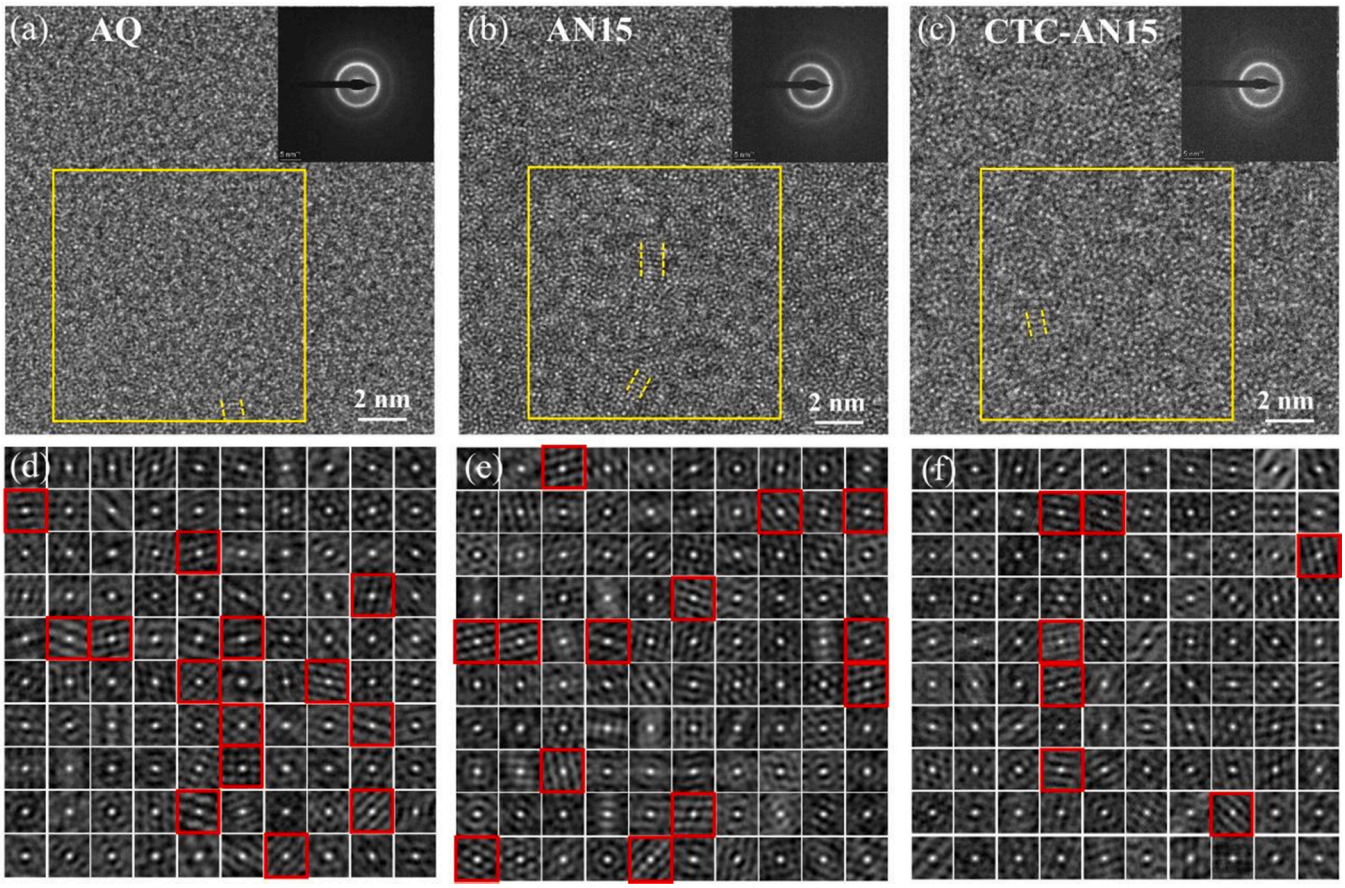

Fig. 7. (a–c) The HRTEM images with corresponding SAED patterns as insets of AQ, AN15, and CTC-AN15 MG samples. The yellow dashed lines highlight the CLO structures. (d–f) The 2D autocorrelation function analysis of the yellow squares in (a–c), respectively.

that the inhomogeneous contrast of AQ and CTC-AN15 samples are more significant, with more dark areas embedded. For AN15 sample, there also exists a large number of dark regions but the size is much smaller. These results indicate that after annealing treatment, the annihilation of free volume is manifested in the reduction of size rather than its quantity. After thermal cycling, the size of soft regions increases significantly, bringing about a more inhomogeneous configuration for CTC-AN15 sample.

4. Discussion

According to the HAADF-STEM and ΔH_{rel} results, the significant deterioration of plastic deformation ability for AN15 sample is mainly due to the smaller size of soft regions. These loosely packed regions with lower stiffness are easier to be activated during deformation, acting as STZs. The smaller size of soft regions facilitates the nucleation of STZs, but is harmful to its percolation when the applied stress continues to increase [33]. Therefore, the initiation and propagation of SBs tend to be difficult, leading to the decreased bending plasticity of samples after annealing treatment. The CTC treatment induces more precipitation of loosely packed structures in the matrix and enhances the energy state of CTC-AN15 sample. These larger soft regions are beneficial to the percolation of STZs and SBs initiation. The massively activated SBs hinder and intersect with each other during propagation, leading to the formation of multiple SBs and energy release, thus the improved plasticity. Nevertheless, the structural inhomogeneity of the CTC-AN15 sample is still lower than the AQ sample, as a large number of free volumes and CLO structures co-exist in AQ sample. The CLO structures of about 1 nm won't cause significant stress concentration because of their small size. Instead, they can serve as obstacles to facilitate the branching and intersection of SBs, suppressing the early failure [13,34,35]. This explains the best bending ability of the AQ sample. It's worth noting that the ε of CTC-AN20 did not increase, which can be attributed to the negligible rejuvenation effect after CTC treatment. After annealing for 20 min, most of the free volumes are annihilated with the ΔH_{rel} decreasing dramatically, and the structure tends to be more homogeneous. In this case, the local stress during thermal cycling is too small to cause large-scale atomic rearrangement, so that the rejuvenation effect is not conspicuous. The initiation and percolation of STZs tends to be difficult because of the small number of soft regions, once the main SB is generated, it will propagate rapidly and lead to fast failure.

In terms of soft magnetic properties, the annealing treatment can effectively release most of the residual stresses in the alloy. It has been reported that the magnetic properties in MGs are closely related to the dynamics of stress relaxation, the unevenly distributed stress will lead to an anisotropic distribution of magnetoelastic energy and thus a more complex domain structure [36]. This can be resolved by short-time annealing. Besides, the annealing treatment promotes the formation of homogeneous and dense structure, which realizes low density of the quasi-dislocation dipole-type elastic stress sources or the low pinning force due to the elastic stress [37]. After annealing treatment, the smaller size of soft regions which contains more voids can reduce the nailing effect on domain walls. Then the domain structures tend to be more uniform and the H_c decreases obviously. For CTC-AN15 sample, although the soft regions become larger compared to the AN15 sample, the number of CLO structures decreases, also reducing the pinning effect on domain walls. The similar phenomenon has also been found in previous report that the magnetic field

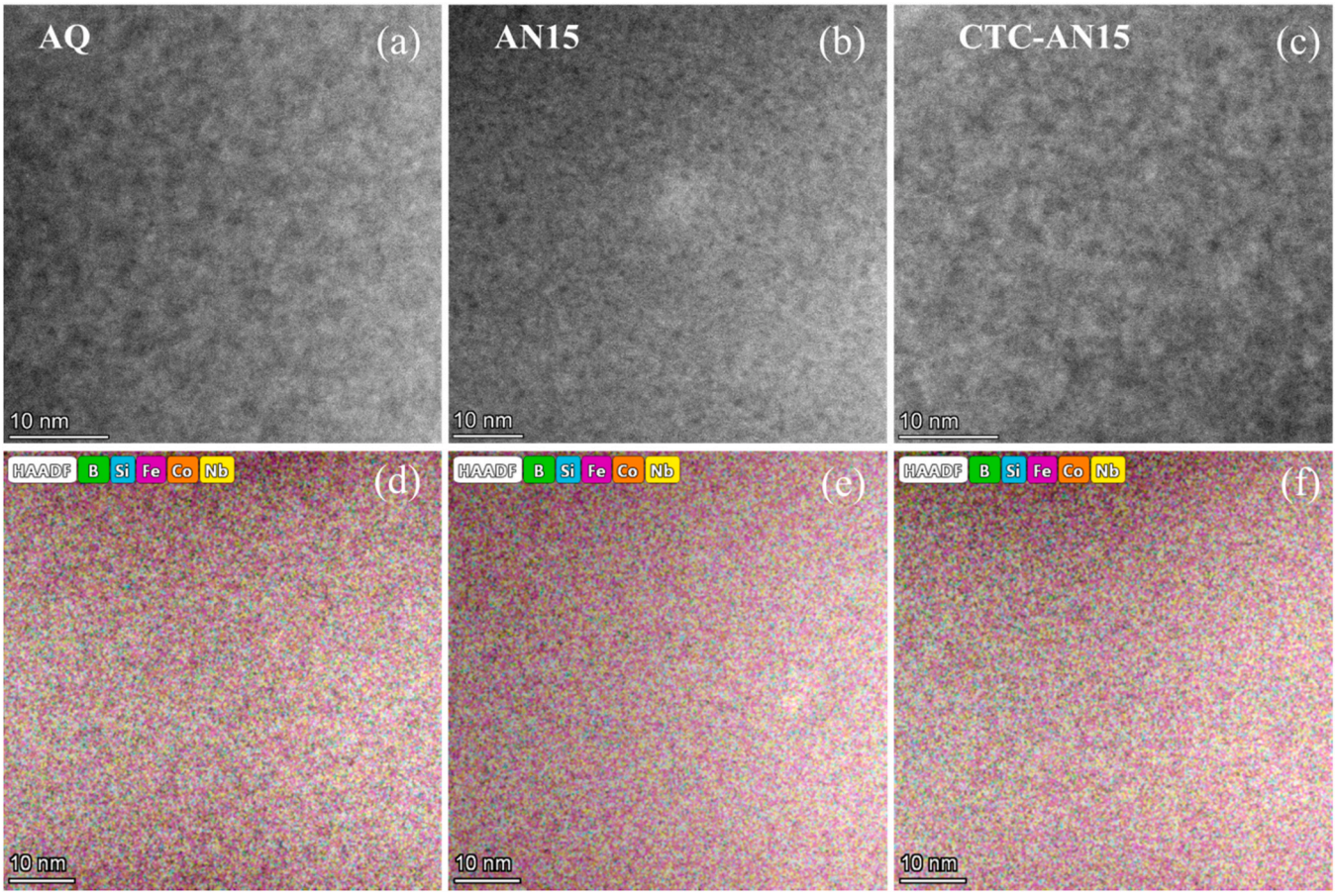

Fig. 8. (a–c) HAADF-HRTEM images and (d–f) the corresponding element mappings of AQ, AN15 and CTC-AN15 samples.

annealing leads to increased ΔH_{rel} but suppressed crystal-like orders, which contributes to the decreased H_c [38]. As a result, the CTC-AN15 sample possesses slightly decreased H_c.

5. Conclusions

The annealing brittleness of $[(Fe_{0.5}Co_{0.5})_{0.75}B_{0.2}Si_{0.05}]_{96}Nb_4$ MG ribbon was effectively reduced by CTC treatment when the annealing time was relatively short. The size of soft regions became larger after thermal cycling, which contributed to the plasticity enhancement. Despite the large soft regions, the number of CLOs decreased obviously after CTC treatment, the domain structure and coercivity of the sample remained nearly identical. Combined with proper annealing and CTC treatment, excellent comprehensive properties with good soft magnetic properties and high bending deformation ability are obtained in the Fe-based MG ribbons. Our results are highly conducive to the processing of Fe-based MGs, effectively reducing the production cost and the number of defective products, and improving the stability and safety of the products. This work can greatly promote and expand the application of Fe-based MGs as soft magnetic material in next-generation electronic devices, high-frequency motors, power supplies, and so on.

CRediT authorship contribution statement

Siyi Di designed the experiments, performed most of the experiments and characterizations. **Mingjuan Cai** and **Xuesong Li** performed the soft magnetic properties measurements. **Jingxian Cui** performed some of the cryogenic thermal cycling treatment. **Qianqian Wang, Haibo Ke, Jing Zhou** and **Baolong Shen** participated in the analyzes of the results. **Siyi Di** wrote the manuscript. **Qianqian Wang and Jing Zhou** revised it. All the authors contributed to the general discussion.

Data Availability

Data will be made available on request.

Declaration of Competing Interest

The authors declare that they have no known competing financial interests or personal relationships that could have appeared to influence the work reported in this paper.

Acknowledgments

This work was supported by National Key R&D Program of China (Grant no. 2022YFB3804100), Jiangsu Provincial Key R&D Program (No. BE2021088) and Fundamental Research Funds for the Central Universities (Grant no. 2242023K40029).

References

[1] Y. Yoshizawa, S. Oguma, K. Yamauchi, New Fe-based soft magnetic alloys composed of ultrafine grain structure, J. Appl. Phys. 64 (1988) 6044–6046, https://doi.org/10.1063/1.342149
[2] X.S. Li, J. Zhou, L.Q. Shen, B.A. Sun, H.Y. Bai, W.H. Wang, Exceptionally high saturation magnetic flux density and ultralow coercivity via an amorphous-nanocrystalline transitional microstructure in an FeCo-Based alloy, Adv. Mater. (2022) 2205863, https://doi.org/10.1002/adma.202205863
[3] M.E. McHenry, M.A. Willard, D.E. Laughlin, Amorphous and nanocrystalline materials for applications as soft magnets, Prog. Mater. Sci. 44 (1999) 291–433, https://doi.org/10.1016/s0079-6425(99)00002-x

[4] J. Dai, Y.G. Wang, X.F. Miao, L. Yang, G.Q. Guo, G.T. Xia, Atomic-scale mechanisms of annealing-induced coercivity modification in metallic glass, J. Mater. Sci. 51 (2016) 8655–8662, https://doi.org/10.1007/s10853-016-0125-z

[5] C. Minnert, M. Kuhnt, S. Bruns, A. Marshal, K.G. Pradeep, M. Marsilius, E. Bruder, K. Durst, Study on the embrittlement of flash annealed $Fe_{85.2}B_{9.5}P_4Cu_{0.8}Si_{0.5}$ metallic glass ribbons, Mater. Des. 156 (2018) 252–261, https://doi.org/10.1016/j.matdes.2018.06.055

[6] H. Zheng, L. Zhu, S.S. Jiang, Y.G. Wang, S.N. Liu, S. Lan, F.G. Chen, Role of Ni and Co in tailoring magnetic and mechanical properties of $Fe_{84}Si_2B_{13}P_1$ metallic glass, J. Alloy. Compd. 816 (2020) 152549, https://doi.org/10.1016/j.jallcom.2019.152549

[7] Y. Meng, S.J. Pang, C.T. Chang, X.Y. Bai, T. Zhang, Nanocrystalline $Fe_{83}Si_4B_{10}P_2Cu_1$ ribbons with improved soft magnetic properties and bend ability prepared via rapid annealing of the amorphous precursor, J. Magn. Magn. Mater. 523 (2021) 167583, https://doi.org/10.1016/j.jmmm.2020.167583

[8] J. Pan, Y.P. Ivanov, W.H. Zhou, Y. Li, A.L. Greer, Strain-hardening and suppression of shear-banding in rejuvenated bulk metallic glass, Nature 578 (2020) 559–562, https://doi.org/10.1038/s41586-020-2016-3

[9] Y.H. Sun, A. Concustell, A.L. Greer, Thermomechanical processing of metallic glasses: extending the range of the glassy state, Nat. Rev. Mater. 1 (2016) 1–14, https://doi.org/10.1038/natrevmats.2016.39

[10] S.V. Ketov, Y.H. Sun, S. Nachum, Z. Lu, A. Checchi, A.R. Beraldin, H.Y. Bai, W.H. Wang, D.V. Louzguine-Luzgin, M.A. Carpenter, A.L. Greer, Rejuvenation of metallic glasses by non-affine thermal strain, Nature 524 (2015) 200–203, https://doi.org/10.1038/nature14674

[11] H. Zheng, L. Zhu, S.S. Jiang, Y.G. Wang, F.G. Chen, Recovering the bending ductility of the stress-relieved Fe-based amorphous alloy ribbons by cryogenic thermal cycling, J. Alloy. Compd. 790 (2019) 529–535, https://doi.org/10.1016/j.jallcom.2019.03.213

[12] S.Y. Di, Q.Q. Wang, Y.Y. Yang, T. Liang, J. Zhou, L. Su, K.B. Yin, Q.S. Zeng, L.T. Sun, B.L. Shen, Efficient rejuvenation of heterogeneous $\{[(Fe_{0.5}Co_{0.5})_{0.75}B_{0.2}Si_{0.05}]_{96}Nb_4\}_{99.9}Cu_{0.1}$ bulk metallic glass upon cryogenic cycling treatment, J. Mater. Sci. Technol. 97 (2022) 20–28, https://doi.org/10.1016/j.jmst.2021.04.034

[13] S.Y. Di, Q.Q. Wang, J. Zhou, Y.Y. Shen, J.Q. Li, M.Y. Zhu, K.B. Yin, Q.S. Zeng, L.T. Sun, B.L. Shen, Enhancement of plasticity for FeCoBSiNb bulk metallic glass with superhigh strength through cryogenic thermal cycling, Scr. Mater. 187 (2020) 13–18, https://doi.org/10.1016/j.scriptamat.2020.05.059

[14] S.Y. Di, H.B. Ke, Q.Q. Wang, J. Zhou, Y. Zhao, B.L. Shen, Large tensile plasticity induced by pronounced β-relaxation in Fe-based metallic glass via cryogenic thermal cycling, Mater. Des. 222 (2022) 111074, https://doi.org/10.1016/j.matdes.2022.111074

[15] S.V. Ketov, A.S. Trifonov, Y.P. Ivanov, A.Y. Churyumov, A.V. Lubenchenko, A.A. Batrakov, J. Jiang, D.V. Louzguine-Luzgin, J. Eckert, J. Orava, A.L. Greer, On cryothermal cycling as a method for inducing structural changes in metallic glasses, NPG Asia Mater. 10 (2018) 137–145, https://doi.org/10.1038/s41427-018-0019-4

[16] W. Guo, J.J. Saida, M. Zhao, S.L. Lü, S.S. Wu, Rejuvenation of Zr-based bulk metallic glass matrix composite upon deep cryogenic cycling, Mater. Lett. 247 (2019) 135–138, https://doi.org/10.1016/j.matlet.2019.03.117

[17] W. Guo, R. Yamada, J. Saida, S. Lu, S. Wu, Various rejuvenation behaviors of Zr-Based metallic glass by cryogenic cycling treatment with different casting temperatures, Nanoscale Res. Lett. 13 (2018) 398, https://doi.org/10.1186/s11671-018-2816-7

[18] S. Sohrabi, M.C. Ri, H.Y. Jiang, L. Gu, P. Wen, Y.H. Sun, W.H. Wang, Prominent role of chemical heterogeneity on cryogenic rejuvenation and thermomechanical properties of La-Al-Ni metallic glass, Intermetallics 111 (2019) 106497, https://doi.org/10.1016/j.intermet.2019.106497

[19] K.J. Laws, D. Granata, J.F. Löffler, Alloy design strategies for sustained ductility in Mg-based amorphous alloys-tackling structural relaxation, Acta Mater. 103 (2016) 735–745, https://doi.org/10.1016/j.actamat.2015.08.077

[20] D.T.A. Matthews, V. Ocelik, P.M. Bronsveld, J.T.M. De Hosson, An electron microscopy appraisal of tensile fracture in metallic glasses, Acta Mater. 56 (2008) 1762–1773, https://doi.org/10.1016/j.actamat.2007.12.029

[21] Z.C. Ma, H.W. Zhao, X.J. Du, X.X. Ma, Z.F. Qiang, F. Zhang, L.M. Zhou, L.Q. Ren, Static and cyclic mechanical behaviours and fracture mechanisms of Zr-based metallic glass at elevated temperatures, Philos. Mag. 99 (2019) 835–852, https://doi.org/10.1080/14786435.2018.1562280

[22] G. Wang, J. Shen, J.F. Sun, Z.P. Lu, Z.H. Stachurski, B.D. Zhou, Tensile fracture characteristics and deformation behavior of a Zr-based bulk metallic glass at high temperatures, Intermetallics 13 (2005) 642–648, https://doi.org/10.1016/j.intermet.2004.10.011

[23] M.E. Dokukin, N.S. Perov, A.I. Beskrovnyi, E.B. Dokukin, Structural relaxation of amorphous metallic alloys, J. Magn. Magn. Mater. 272 (2004) E1151–E1152, https://doi.org/10.1016/j.jmmm.2003.12.1095

[24] M. Tejedor, J.A. Garcia, J. Carrizo, L. Elbaile, Mechanical determination of internal stresses in as-quenched magnetic amorphous metallic ribbons, J. Mater. Sci. 32 (1997) 2337–2340, https://doi.org/10.1023/A:1018536603243

[25] X.B. Liang, T. Kulik, J. Ference, M. Kowalczyk, G. Vlasak, W.S. Sun, B.S. Xu, Influence of structure on coercivity in nanocrystalline $(Fe_{1-x}Co_x)_{86}Hf_7B_6Cu_1$ alloys, Physica B 370 (2005) 151–157, https://doi.org/10.1016/j.physb.2005.09.005

[26] B.R. Sun, S.W. Xin, T.D. Shen, Microstructural origin of the ultra-low coercivity in bulk $Fe_{65.5}Cr_4Mo_4Ga_4P_{12}B_{5.5}C_5$ metallic glasses, J. Magn. Magn. Mater. 466 (2018) 130–132, https://doi.org/10.1016/j.jmmm.2018.06.083

[27] L.Y. Chen, A.D. Setyawan, H. Kato, A. Inoue, G.Q. Zhang, J. Saida, X.D. Wang, Q.P. Cao, J.Z. Jiang, Free-volume-induced enhancement of plasticity in a monolithic bulk metallic glass at room temperature, Scr. Mater. 59 (2008) 75–78, https://doi.org/10.1016/j.scriptamat.2008.02.025

[28] H. Guo, C.B. Jiang, B.J. Yang, J.Q. Wang, Deformation behavior of Al-rich metallic glasses under nanoindentation, J. Mater. Sci. Technol. 33 (2017) 1272–1277, https://doi.org/10.1016/j.jmst.2016.10.014

[29] Q. Wang, C.T. Liu, Y. Yang, J.B. Liu, Y.D. Dong, J. Lu, The atomic-scale mechanism for the enhanced glass-forming-ability of a Cu-Zr based bulk metallic glass with minor element additions, Sci. Rep. 4 (2014) 4648, https://doi.org/10.1038/srep04648

[30] X.J. Liu, G.L. Chen, H.Y. Hou, X. Hui, K.F. Yao, Z.P. Lu, C.T. Liu, Atomistic mechanism for nanocrystallization of metallic glasses, Acta Mater. 56 (2008) 2760–2769, https://doi.org/10.1016/j.actamat.2008.02.019

[31] Q. Hu, J.M. Wang, Y.H. Yan, S. Guo, S.S. Chen, D.P. Lu, J.Z. Zou, X.R. Zeng, Invar effect of Fe-based bulk metallic glasses, Intermetallics 93 (2018) 318–322, https://doi.org/10.1016/j.intermet.2017.10.012

[32] F. Zhu, A. Hirata, P. Liu, S.X. Song, Y. Tian, J.H. Han, T. Fujita, M.W. Chen, Correlation between local structure order and spatial heterogeneity in a metallic glass, Phys. Rev. Lett. 119 (2017) 215501, https://doi.org/10.1103/PhysRevLett.119.215501 215501.

[33] Z.Q. Chen, L. Huang, P. Huang, K.W. Xu, F. Wang, T.J. Lu, Clarification on shear transformation zone size and its correlation with plasticity for Zr-based bulk metallic glass in different structural states, Mater. Sci. Eng. A 677 (2016) 349–355, https://doi.org/10.1016/j.msea.2016.09.054

[34] B. Sarac, Y.P. Ivanov, A. Chuvilin, T. Schöberl, M. Stoica, Z.L. Zhang, J. Eckert, Origin of large plasticity and multiscale effects in iron-based metallic glasses, Nat. Commun. 9 (2018) 1333, https://doi.org/10.1038/s41467-018-03744-5

[35] J. Zhou, Q.Q. Wang, X.D. Hui, Q.S. Zeng, Y.W. Xiong, K.B. Yin, B.A. Sun, L.T. Sun, M. Stoica, W.H. Wang, B.L. Shen, A novel FeNi-based bulk metallic glass with high notch toughness over 70 MPa $m^{1/2}$ combined with excellent soft magnetic properties, Mater. Des. 191 (2020) 108597, https://doi.org/10.1016/j.matdes.2020.108597

[36] R. Williams, T. Egami, Effects of deformation and annealing on magnetic amorphous alloys, IEEE Trans. Magn. 12 (1976) 927–929, https://doi.org/10.1109/TMAG.1976.1059247

[37] T. Bitoh, A. Makino, A. Inoue, Origin of low coercivity of Fe-(Al, Ga)-(P, C, B, Si, Ge) bulk glassy alloys, Mater. Trans. 44 (2003) 2020–2024, https://doi.org/10.2320/matertrans.44.2020

[38] Q. Luo, D.H. Li, M.J. Cai, S.Y. Di, Z.G. Zhang, Q.S. Zeng, Q.Q. Wang, B.L. Shen, Excellent magnetic softness-magnetization synergy and suppressed defect activation in soft magnetic amorphous alloys by magnetic field annealing, J. Mater. Sci. Technol. 116 (2022) 72–82, https://doi.org/10.1016/j.jmst.2021.11.038